

Supplementary Information

## Tuning the Dual Emissions of a Monoruthenium Complex with a Dangling Coordination Site by Solvents, O<sub>2</sub>, and Metal Ions

Si-Hai Wu,<sup>\*a</sup> Jiang-Yang Shao,<sup>b</sup> Zhong-Liang Gong,<sup>b</sup> Na Chen,<sup>a</sup> and Yu-Wu Zhong<sup>\*b,c</sup>

<sup>a</sup>School of Biomedical Sciences, Huaqiao University, Quanzhou, Fujian 362021, China. E-mail: [wusihai@hqu.edu.cn](mailto:wusihai@hqu.edu.cn)

<sup>b</sup>CAS Key Laboratory of Photochemistry, CAS Research/Education Center for Excellence in Molecular Sciences, Institute of Chemistry, Chinese Academy of Sciences, Beijing 100190, China. E-mail: [zhongyuwu@iccas.ac.cn](mailto:zhongyuwu@iccas.ac.cn)

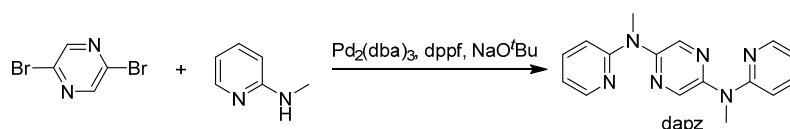
<sup>c</sup>University of Chinese Academy of Sciences Beijing 100049, China

### Contents

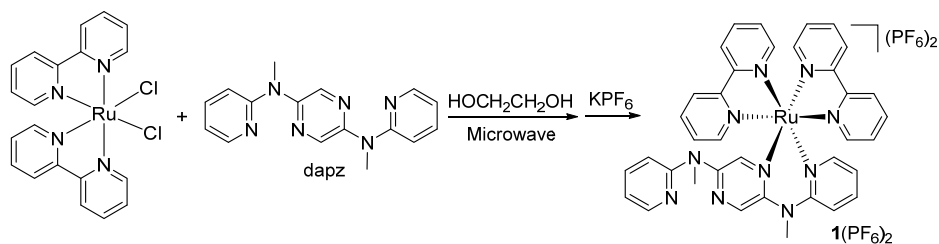
1. Synthesis and Characterization
2. HPLC Analysis
3. Single-Crystal X-Ray Analysis
4. Spectroscopic Analysis
5. Emission Lifetime Analysis
6. DFT and TDDFT Calculations
7. Electrochemical Measurements

## 1. Synthesis and Characterization

**General.** NMR spectra were recorded in the designated solvent on a Bruker Avance spectrometer. Spectra are reported in ppm values from residual protons of the deuterated solvent for  $^1\text{H}$  NMR (7.26 ppm for  $\text{CDCl}_3$  and 1.92 ppm for  $\text{CD}_3\text{CN}$ ). Mass data were obtained with a Bruker Daltonics Inc. Apex II FT-ICR or Autoflex III MALDI-TOF mass spectrometer. The matrix for matrix-assisted laser desorption ionization time-of-flight (MALDI-TOF) measurement is  $\alpha$ -cyano-4-hydroxycinnamic acid. Microanalysis was carried out using a Flash EA 1112 or Carlo Erba 1106 analyzer at the Institute of Chemistry, Chinese Academy of Sciences.



**Synthesis of 2,5-di(*N*-methyl-*N'*-(pyrid-2-yl)amino)pyrazine (dapz).** A suspension of 2,5-dibromopyrazine (476 mg, 2.0 mmol), 2-(methylamino)pyridine (475 mg, 4.4 mmol), tris(dibenzylideneacetone)dipalladium ( $\text{Pd}_2(\text{dba})_3$ , 183 mg, 0.20 mmol), 1,1'-bis(diphenylphosphino)ferrocene (dppf, 110 mg, 0.20 mmol), and  $\text{NaO}^t\text{Bu}$  (768 mg, 8.0 mmol) in 15 mL of dry toluene was heated at 130 °C for 48 h under nitrogen atmosphere. The resulting mixture was cooled to room temperature. The solvent was removed under reduced pressure and the crude product was purified by column chromatography on silica gel (eluent with petroleum ether/ethyl acetate 3/1) to afford 576 mg of dapz as a yellow solid in 98% yield.  $^1\text{H}$  NMR (300 MHz,  $\text{CDCl}_3$ ):  $\delta$  3.59 (s, 6H), 6.85 (t,  $J = 6.0$  Hz, 2H), 7.03 (d,  $J = 8.4$  Hz, 2H), 7.55 (t,  $J = 8.0$  Hz, 2H), 8.31 (d,  $J = 4.8$  Hz, 2H), 8.45 (s, 2H).  $^{13}\text{C}$  NMR (100 MHz,  $\text{CDCl}_3$ ):  $\delta$  36.16, 112.30, 116.73, 136.16, 137.74, 148.30, 148.62, 157.52. EI-MS ( $m/z$ ): 292 for  $[\text{M}]^+$ . ESI-HRMS calcd for  $\text{C}_{16}\text{H}_{17}\text{N}_6$ : 293.150921. Found: 293.150904.



**Synthesis of Complex [(bpy)<sub>2</sub>Ru(dapz)](PF<sub>6</sub>)<sub>2</sub>, **1**(PF<sub>6</sub>)<sub>2</sub>.** To a solution of *cis*-[(bpy)<sub>2</sub>RuCl<sub>2</sub>] (103.8 mg, 0.20 mmol) in 8 mL of ethylene glycol was added the above synthesized ligand dapz (58.4 mg, 0.20 mmol). The resulting mixture was heated under microwave irradiation for 0.5 h (power = 325 W). After cooling to room temperature, an excess of an aqueous solution of KPF<sub>6</sub> was added. The resulting precipitate was collected and purified by flash column chromatography on silica gel using CH<sub>3</sub>CN/KNO<sub>3</sub> (aq.) (200/1) as the eluent to give 177 mg of **1**(PF<sub>6</sub>)<sub>2</sub> as an orange solid in 88% yield. <sup>1</sup>H NMR (400 MHz, CD<sub>3</sub>CN): δ 3.37 (s, 3H), 3.47 (s, 3H), 6.81-6.86 (m, 2H), 6.96 (dd, *J* = 5.2, 2.0 Hz, 1H), 7.17 (t, *J* = 6.0 Hz, 1H), 7.28-7.33 (m, 2H), 7.39 (d, *J* = 4.0 Hz, 1H), 7.59-7.61 (m, 6H), 7.79-7.84 (m, 2H), 7.89 (t, *J* = 8.0 Hz, 1H), 7.94 (t, *J* = 8.0 Hz, 1H), 8.12 (t, *J* = 8.0 Hz, 1H), 8.16 (t, *J* = 8.0 Hz, 1H), 8.32-8.36 (m, 4H), 8.41 (d, *J* = 8.0 Hz, 1H), 8.51 (d, *J* = 8.4 Hz, 1H), 8.58 (d, *J* = 5.6 Hz, 1H). <sup>13</sup>C NMR (100 MHz, CD<sub>3</sub>CN): δ 36.40, 41.44, 115.11, 116.78, 120.03, 121.66, 125.44, 125.54, 125.63, 125.94, 128.01, 128.51, 128.55, 128.89, 136.45, 136.95, 138.96, 139.12, 139.46, 139.54, 140.14, 140.84, 147.78, 149.06, 151.02, 152.12, 153.09, 153.23, 154.15, 154.64, 157.38, 158.51, 158.54, 158.56, 158.64, 160.05. MALDI-MS (*m/z*): 708.2 for [M – 2PF<sub>6</sub>]<sup>+</sup>, 548.1 for [M – 2PF<sub>6</sub> – bpy]<sup>+</sup>. Anal. Calcd for C<sub>36</sub>H<sub>32</sub>F<sub>12</sub>N<sub>10</sub>P<sub>2</sub>Ru·H<sub>2</sub>O: C, 42.65; H, 3.38; N, 13.82. Found: C, 42.68; H, 3.73; N, 13.72.

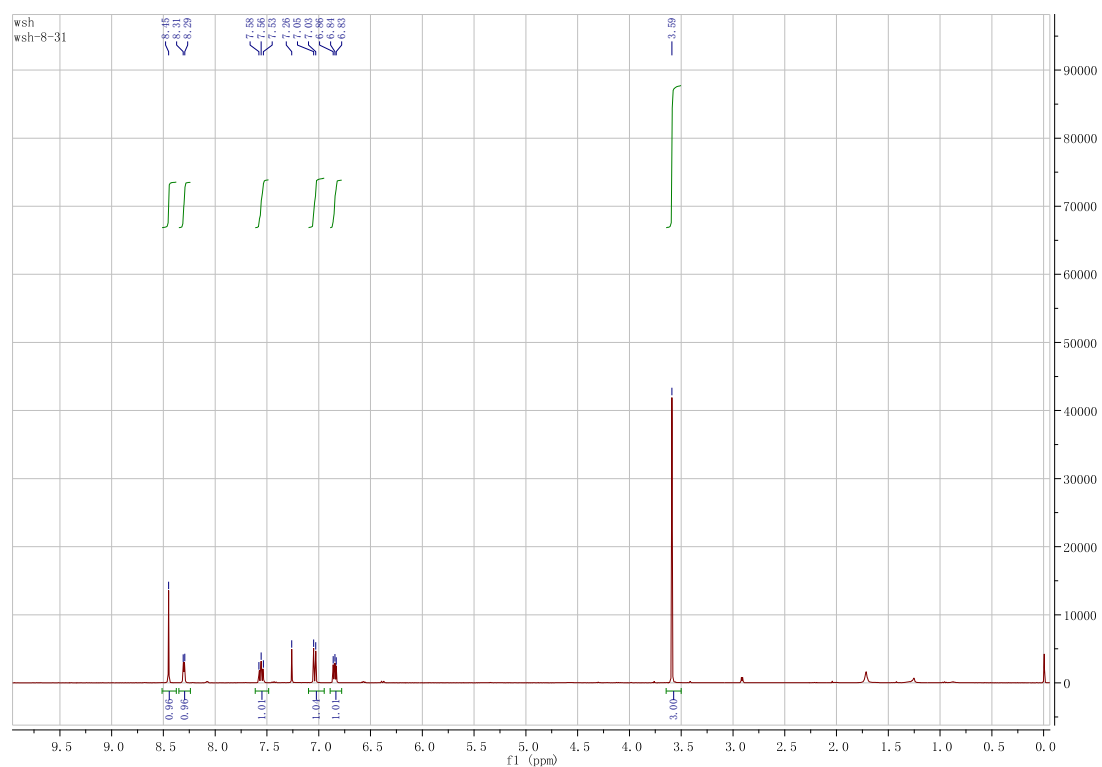


**Figure S1.**  $^1\text{H}$  NMR spectrum of dapz in  $\text{CDCl}_3$ .

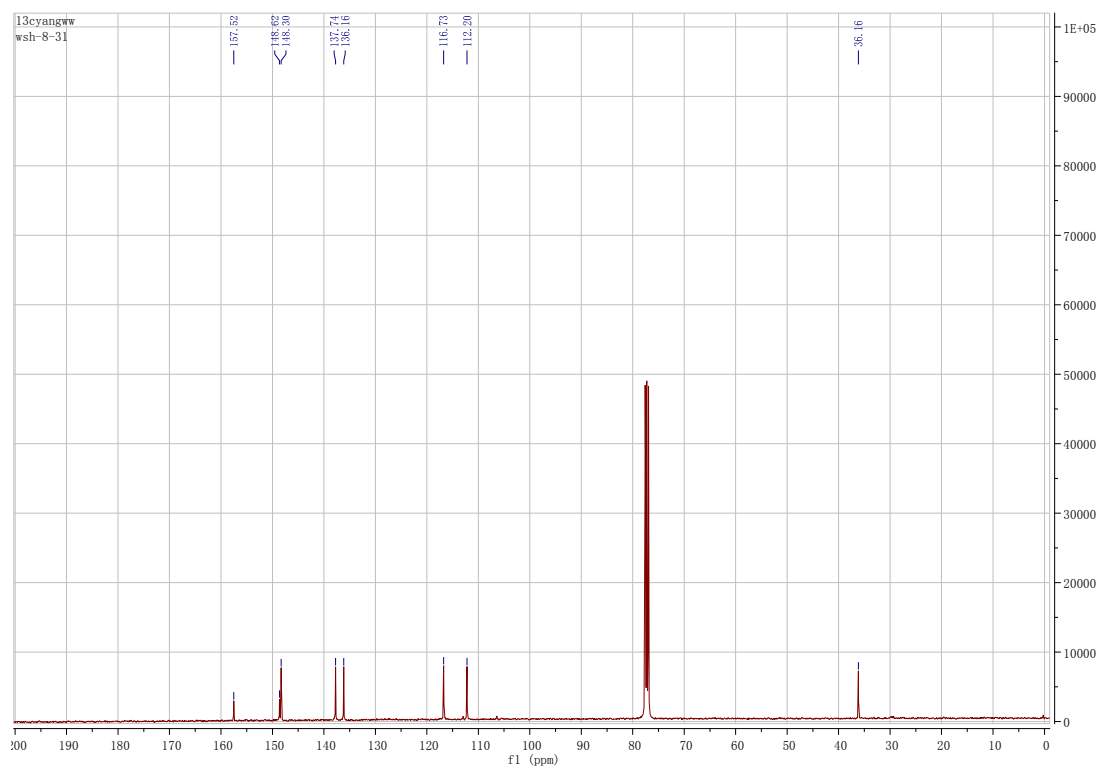


**Figure S2.**  $^{13}\text{C}$  NMR spectrum of dapz in  $\text{CDCl}_3$ .



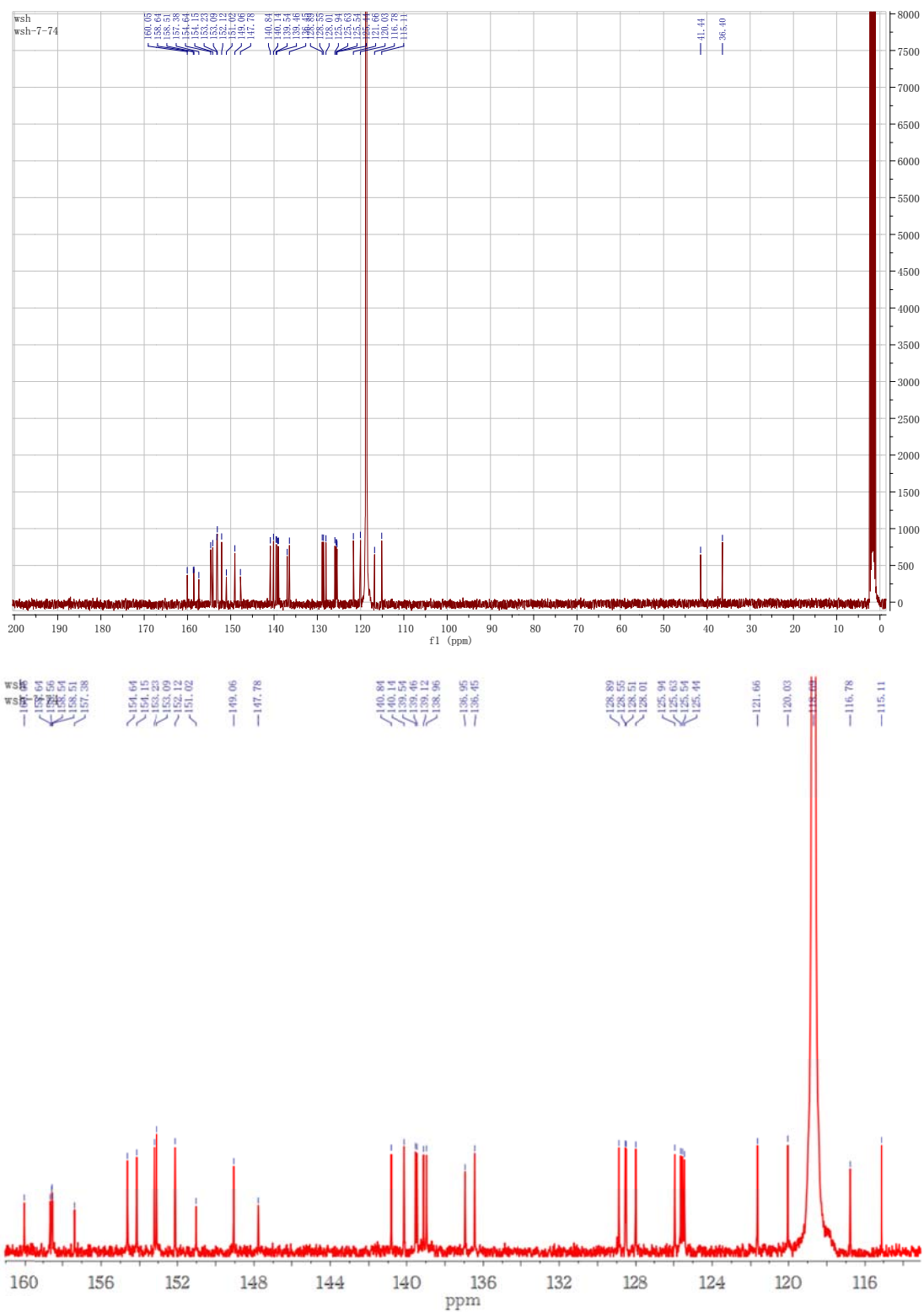


**Figure S4.**  $^{13}\text{C}$  NMR spectrum of  $1(\text{PF}_6)_2$  in  $\text{CD}_3\text{CN}$ .

## 2. HPLC Analysis

HPLC analysis was performed on a Shimadzu UFLC system consisting of two LC-20AD pumps, a SPD-M20A diode array detector, a CTO-20A oven, and a SIL-20A autosampler. HPLC grade solvents were obtained from Fisher Scientific. A Shim-pack XR-ODS (Shimadzu, Japan) column (2.2  $\mu\text{m}$ , 75 mm  $\times$  4.6 mm, i.d.) was used for the analysis. Compounds were eluted with a gradient solvent of  $\text{CH}_3\text{CN}$  in water (10-90% over 0-10 min, followed by isocratic elution of 90%  $\text{CH}_3\text{CN}$  for 5 min. All solvents contain 0.1% of TFA. The flow rate was 1.0 mL/min. The detection wavelengths were set at 360 nm and 450 nm for ligand dapz and complex **1**( $\text{PF}_6$ )<sub>2</sub>, respectively.

### 3. Single-Crystal X-Ray Analysis

The X-ray diffraction data were collected using a Rigaku Saturn 724 diffractometer on a rotating anode (Mo-K radiation, 0.71073 Å) at 173 K. The structure was solved using SHELXS-97<sup>1</sup> and refined with Olex2.<sup>2</sup> The structure graphics were generated using Olex2.

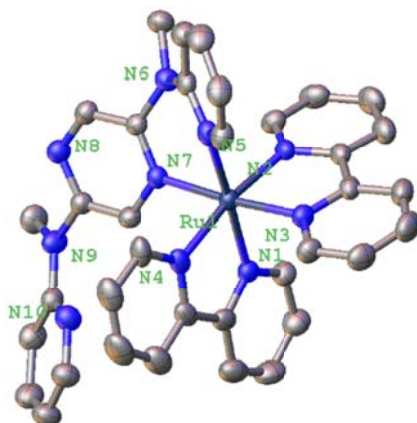
**Table S1.** Crystallographic data of **1**(PF<sub>6</sub>)<sub>2</sub>.

compound	<b>1</b> (PF <sub>6</sub> ) <sub>2</sub>
CCDC number	1570857
empirical formula	C <sub>38</sub> H <sub>32</sub> F <sub>12</sub> N <sub>10</sub> P <sub>2</sub> Ru·(CH <sub>2</sub> Cl <sub>2</sub> ) <sub>2</sub>
formula weight	1165.58
crystal system	triclinic
a (Å)	12.158(2)
b (Å)	12.408(3)
c (Å)	15.666(3)
V (Å <sup>3</sup> )	2225.7(9)
α (°)	76.75(3)
β (°)	85.54(3)
γ (°)	75.42(3)
Z value	2
Density (g/cm <sup>3</sup> )	1.739
R1 (final)	0.0841
wR2 (final)	0.2209
R1 (all)	0.0879
wR2 (all)	0.2247

<sup>1</sup> Sheldrick, G. M. *Acta Cryst.* **2008**, *A64*, 112.

<sup>2</sup> Dolomanov, O. V.; Bourhis, L. J.; Gildea, R. J.; Howard, J. A. K.; Puschmann, H. *J. Appl. Cryst.* **2009**, *42*, 339.

**Table S2.** Selected Bond Lengths and Bond Angles



compound	bond lengths (Å)		bond angles (°)	
<b>1</b> (PF <sub>6</sub> ) <sub>2</sub>	Ru(1)-N(1)	2.062(4)	N(1)-Ru(1)-N(4)	78.87(18)
	Ru(1)-N(2)	2.063(4)	N(2)-Ru(1)-N(3)	79.01(17)
	Ru(1)-N(3)	2.067(4)	N(2)-Ru(1)-N(5)	91.92(16)
	Ru(1)-N(4)	2.066(4)	N(3)-Ru(1)-N(5)	91.68(17)
	Ru(1)-N(5)	2.108(4)	N(4)-Ru(1)-N(5)	96.37(17)
	Ru(1)-N(7)	2.070(4)	N(5)-Ru(1)-N(7)	86.59(16)

#### 4. Spectroscopic Analysis

All optical absorption spectra were obtained using a TU-1810DSPC spectrometer of Beijing Purkinje General Instrument Co. Ltd. at room temperature in denoted solvents, with a conventional 1.0 cm quartz cell.

Emission spectra were recorded using a F-380 spectrofluorimeter of Tianjin Gangdong Sic. & Tech Development Co. Ltd, with a red-sensitive photomultiplier tube R928F. Samples for emission measurement were obtained within quartz cuvettes of 1 cm path length. Luminescence quantum yields were determined using quinine sulfate in 1.0 M aq H<sub>2</sub>SO<sub>4</sub> ( $\Phi = 55\%$ ) or [Ru(bpy)<sub>3</sub>](PF<sub>6</sub>)<sub>2</sub> ( $\Phi = 9.5\%$ ) in degassed acetonitrile solution as the standard; estimated uncertainty of  $\phi$  is  $\pm 10\%$  or better.

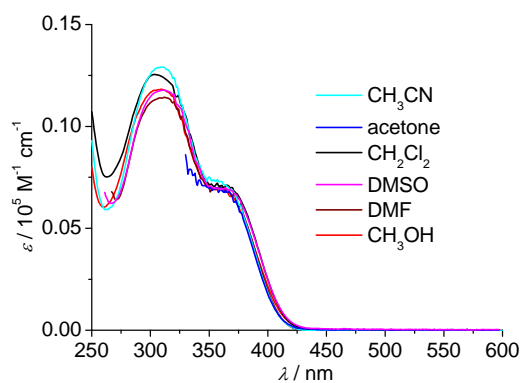


**Figure S5.** Absorption spectra of dapz in different solvents.

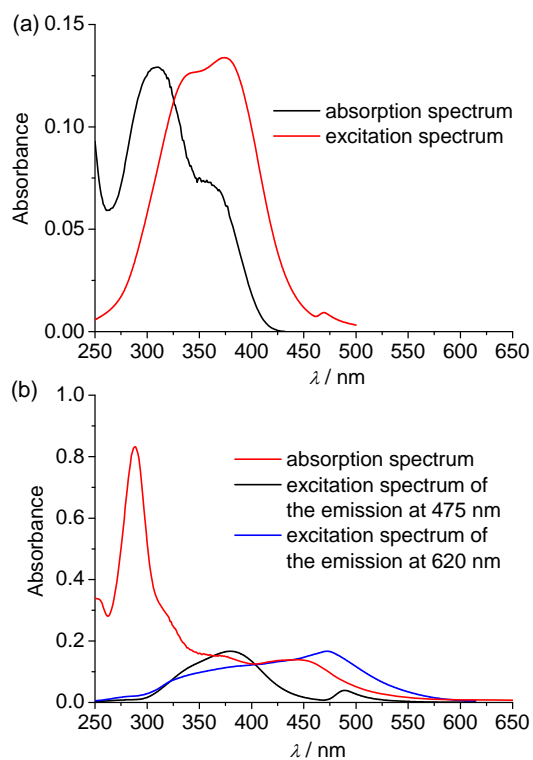


**Figure S6.** (a) Excitation spectrum of dapz in  $\text{CH}_3\text{CN}$ , monitoring for the emission centered at 460 nm. (b) Excitation spectra for  $\mathbf{1}(\text{PF}_6)_2$  in  $\text{CH}_3\text{CN}$ , monitoring for emission centered at 475 nm and 620 nm, respectively. The absorption spectra of two compounds are included for comparison.

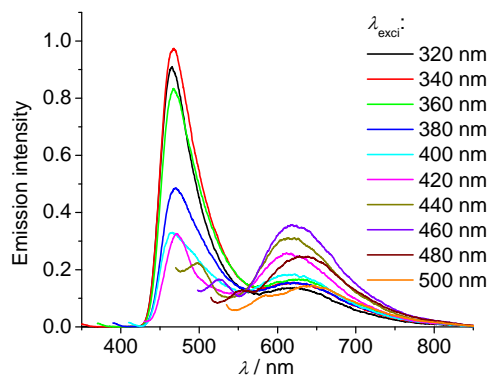


**Figure S7.** Emission spectra of  $\mathbf{1}(\text{PF}_6)_2$  in  $\text{CH}_3\text{CN}$  at the excitation of different wavelength ( $\lambda_{\text{exci}}$ ).

## 5. Emission Lifetime Analysis

The luminescence decays were measured using a nanosecond flash photolysis setup Edinburgh LP920 spectrometer (Edinburgh Instruments Ltd.), combined with a Nd:YAG laser (Surelite II, Continuum Inc.). The sample was excited by a 355 nm laser pulse (1 Hz, 15 mJ/pulse, fwhm  $\approx$  7 ns). A monochromator equipped with a photomultiplier for collecting the spectral range from 300 to 850 nm was used to analyze the luminescence decays. Data were analyzed by the online software of the LP920 spectrophotometer.

**Table S3.** Emission lifetime data of **1**(PF<sub>6</sub>)<sub>2</sub> in different solvents.<sup>a</sup>

Solvent	$\tau$ [ns] (N <sub>2</sub> -saturated)			$\tau$ [ns] (air-equilibrated)		
	$\tau_1$ (A <sub>1</sub> )	$\tau_2$ (A <sub>2</sub> )	$\tau_{av}$	$\tau_1$ (A <sub>1</sub> )	$\tau_2$ (A <sub>2</sub> )	$\tau_{av}$
CH <sub>3</sub> CN	16 (0.038)	219 (0.006)	155	15 (0.014)	58 (0.015)	49
acetone	20 (0.018)	137 (0.0065)	103	17 (0.01)	63 (0.0093)	53
CH <sub>2</sub> Cl <sub>2</sub>	27 (0.016)	136 (0.024)	74	17 (0.025)	93 (0.0088)	67
DMSO	--	--	162	--	--	146
DMF	--	--	122	--	--	81
MeOH	--	--	52	--	--	42

<sup>a</sup>Measured at rt at 10<sup>-5</sup> M. Excited at 355 nm. Detection wavelength is 625 nm. The data measured in CH<sub>3</sub>CN, acetone, and CH<sub>2</sub>Cl<sub>2</sub> is simulated by a biexponential decay, where the shorter component  $\tau_1$  is very likely from the excitation laser source (lifetime around 20 ns). The emissions at 625 nm in these solvents are relatively weaker. The longer component  $\tau_1$  is reported in Table 1 in the main article, which is believed to be associated with the true emission at 625 nm. The data measured in DMSO, DMF, and MeOH is well simulated by a monoexponential decay. In case of biexponential decay, the average lifetime ( $\tau_{av}$ ) is given for comparison.  $\tau_{av} = [A_1(\tau_1)^2 + A_2(\tau_2)^2]/(A_1\tau_1 + A_2\tau_2)$ .

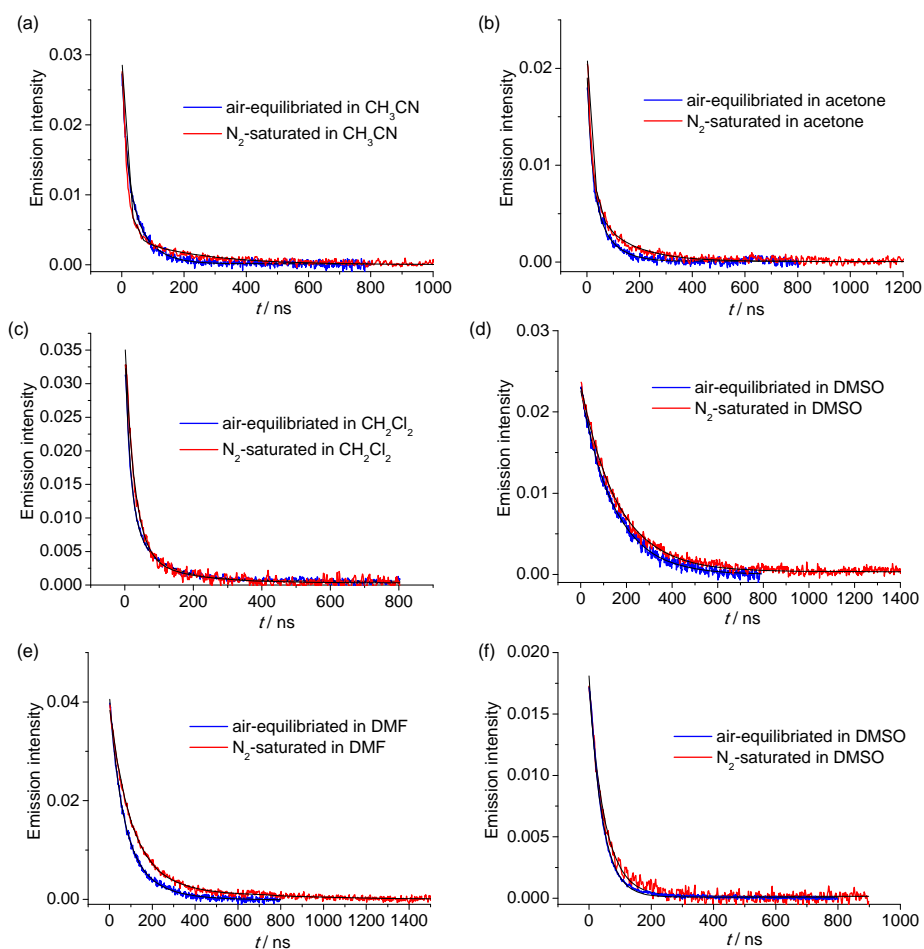


**Figure S8.** Emission decay and simulated curve (black curves) of  $1(\text{PF}_6)_2$  in different air-equilibrated (blue curves) or  $\text{N}_2$ -saturated (red curves) solvents.

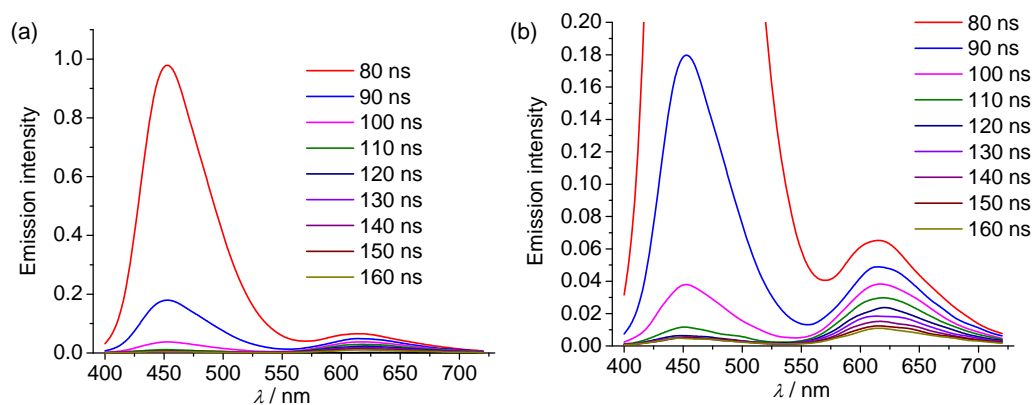


**Figure S9.** Transition emission spectra of  $1(\text{PF}_6)_2$  in  $\text{CH}_3\text{CN}$  at room temperature measured by a nanosecond flash photolysis setup using the Edinburgh LP920 spectrometer. Panel (b) shows the enlarged plots of (a).

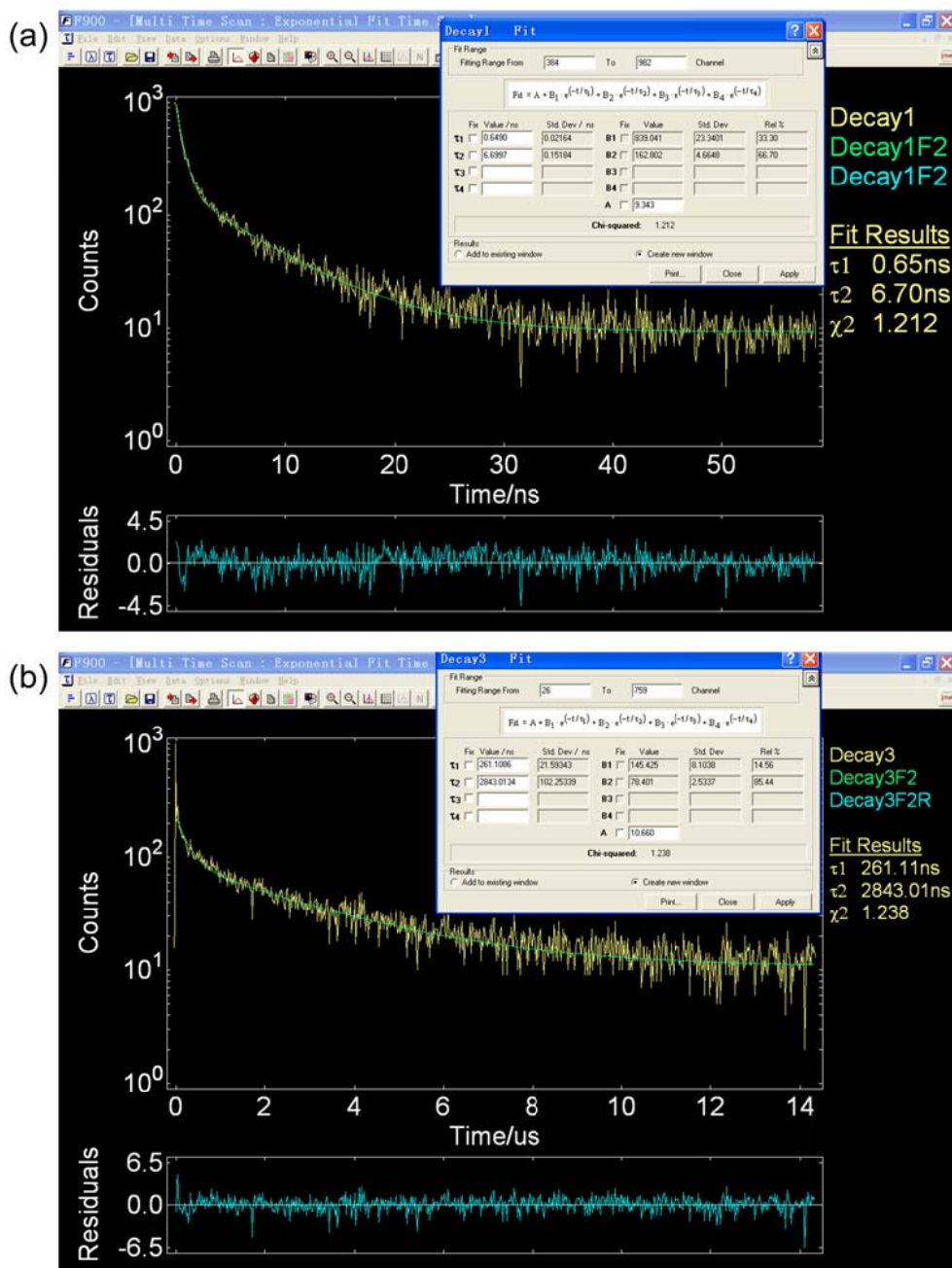


**Figure S10.** Screen shots captured during the lifetime measurement of  $\mathbf{1}(\text{PF}_6)_2$  in glassy  $\text{CH}_3\text{CN}$  at 77 K for the emission band at (a) 450 and (b) 620 nm. Both data were simulated by a monoexponential decay.

The average lifetime  $\tau_{\text{av}}$  was calculated by  $\tau_{\text{av}} = [A_1(\tau_1)^2 + A_2(\tau_2)^2]/(A_1\tau_1 + A_2\tau_2)$ .

For the emission band at (a) 450 nm:  $\tau_1 = 0.65$  ns,  $A_1 = 839$ ,  $\tau_2 = 6.70$  ns,  $A_2 = 163$ ,  $\tau_{\text{av}} = 4.7$  ns.

For the emission band at (b) 620 nm:  $\tau_1 = 261$  ns,  $A_1 = 145$ ,  $\tau_2 = 2843$  ns,  $A_2 = 78$ ,  $\tau_{\text{av}} = 2.5$   $\mu\text{s}$ .

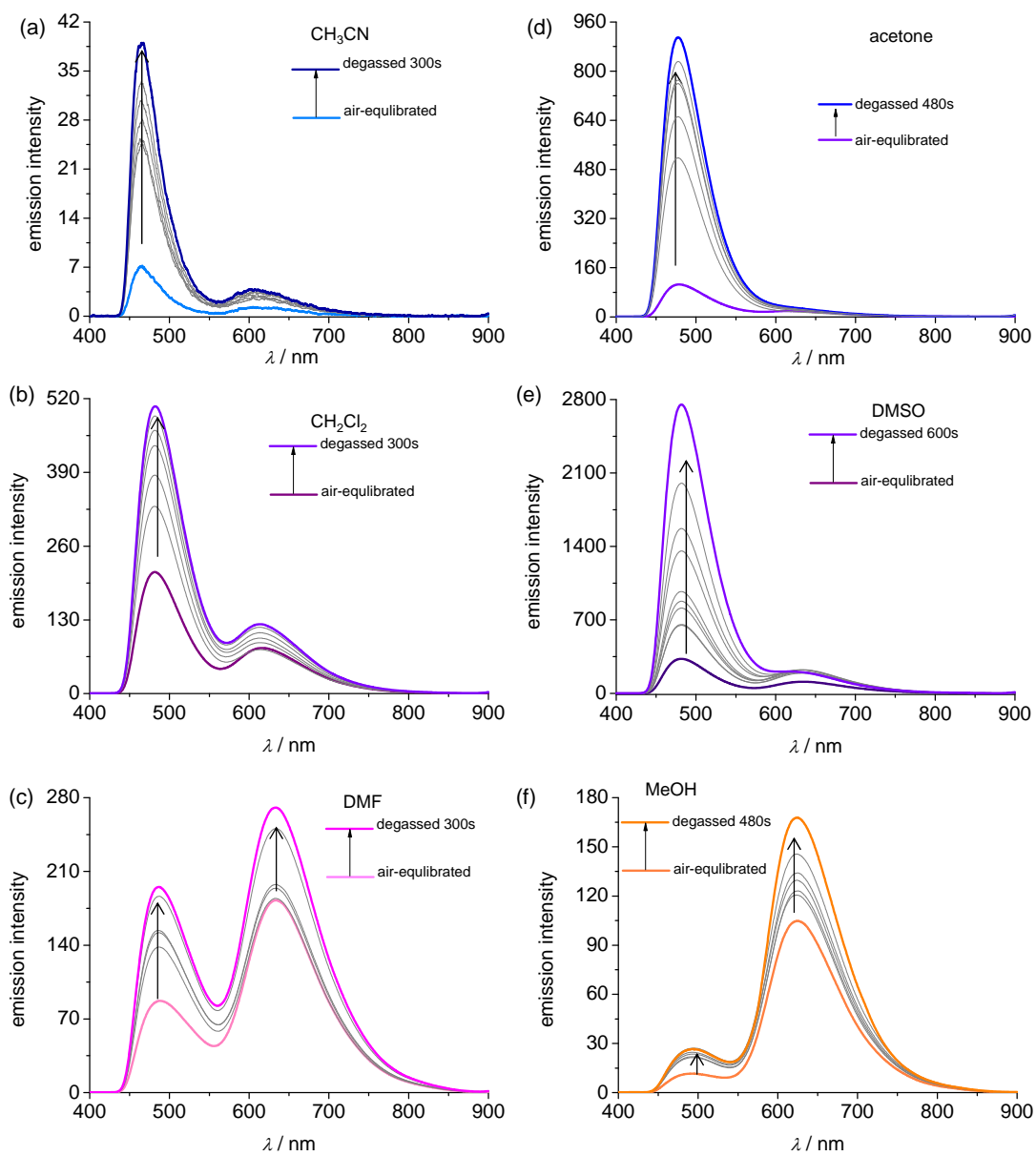


**Figure S11.** Emission spectral changes of air-equilibrated solution of  $1(\text{PF}_6)_2$  in different solvents upon bubbling with  $\text{N}_2$ . Excited at 360 nm for all.

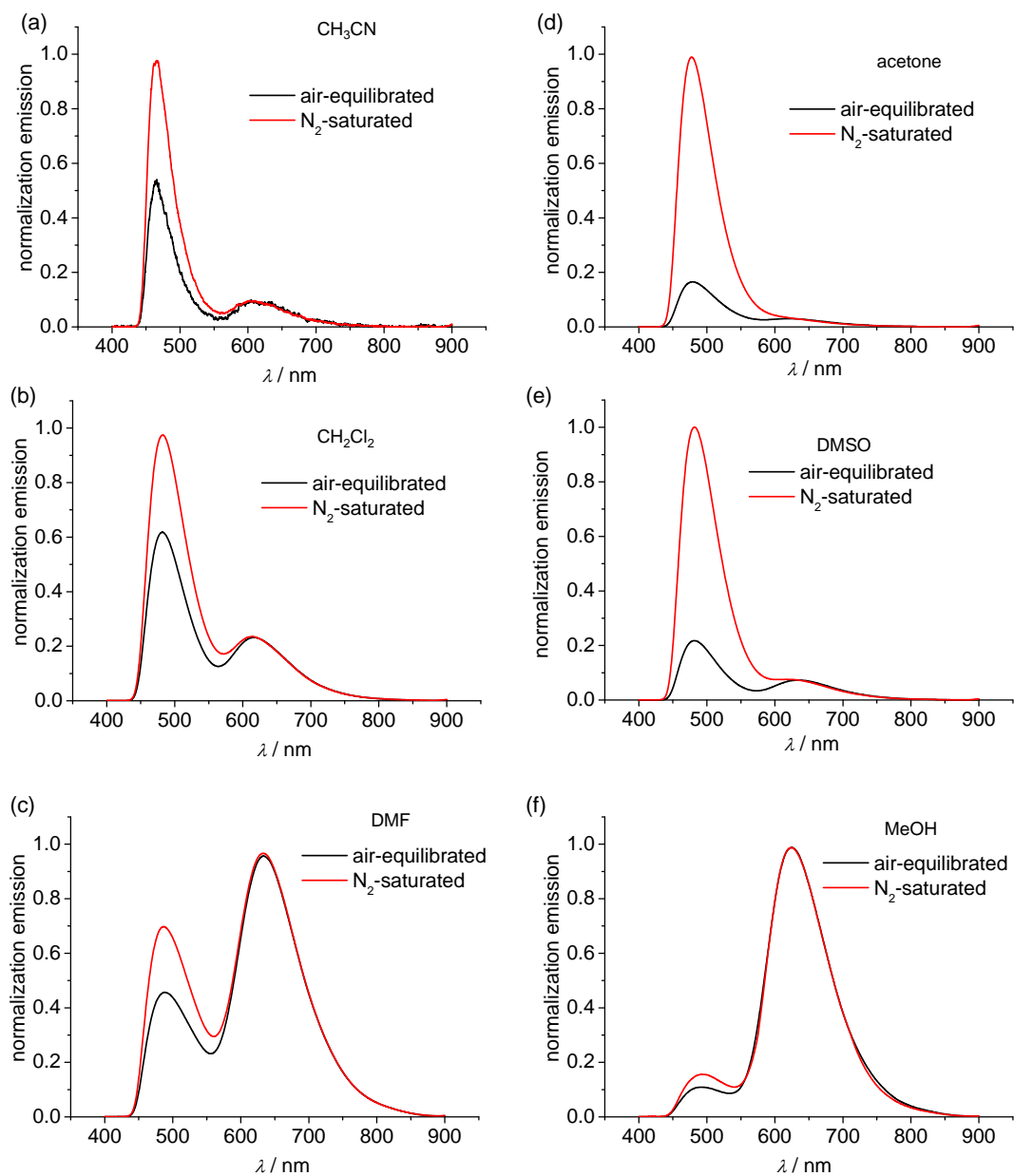


**Figure S12.** Normalized emission spectra of  $1(\text{PF}_6)_2$  (normalized to the emission band at 640 nm) in air-equilibrated or  $\text{N}_2$ -saturated solution. Excited at 360 nm for all.

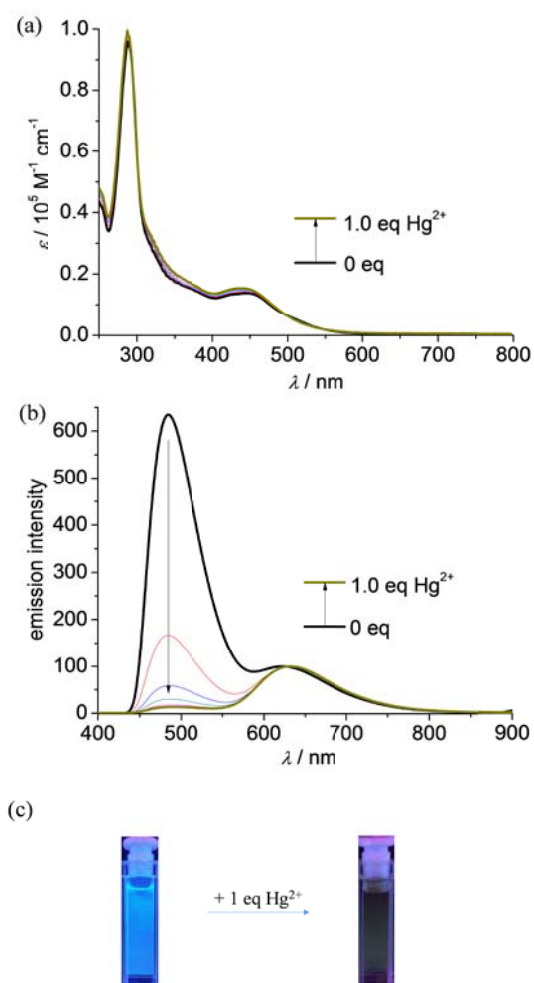


**Figure S13.** (a) Absorption spectral, (b) emission spectral, and (c) emission color (under 365 nm irradiation) changes of  $\mathbf{1}(\text{PF}_6)_2$  ( $5 \times 10^{-5} \text{ M}$  in  $\text{CH}_3\text{CN}$ , 298 K) upon the addition of  $\text{Hg}(\text{ClO}_4)_2$ .

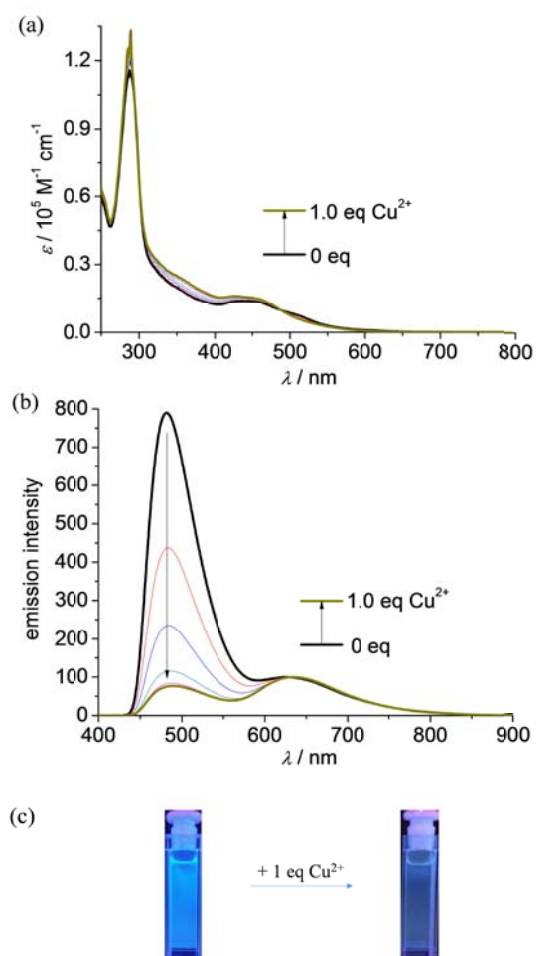


**Figure S14.** (a) Absorption spectral, (b) emission spectral, and (c) emission color (under 365 nm irradiation) changes of  $\mathbf{1}(\text{PF}_6)_2$  ( $5 \times 10^{-5} \text{ M}$  in  $\text{CH}_3\text{CN}$ , 298 K) upon the addition of  $\text{Cu}(\text{ClO}_4)_2$ .

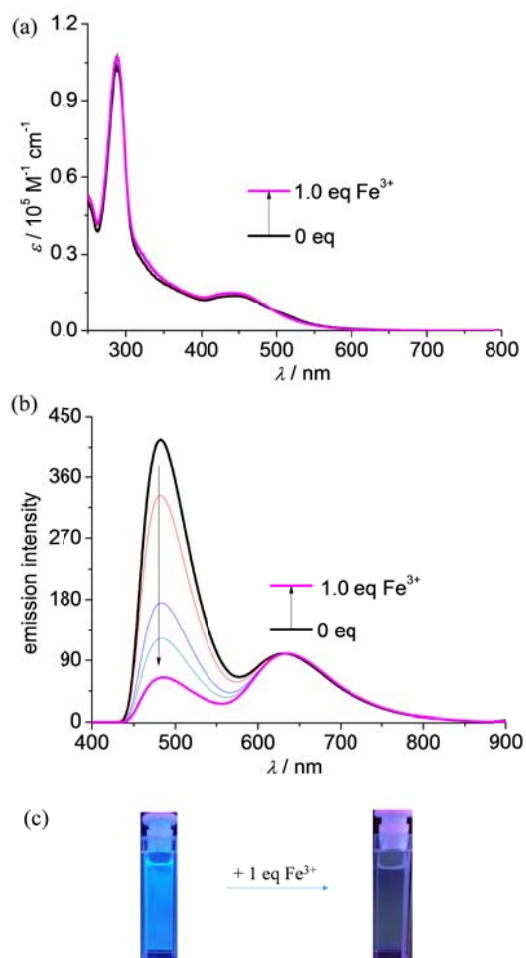


**Figure S15.** (a) Absorption spectral, (b) emission spectral, and (c) emission color (under 365 nm irradiation) changes of  $\mathbf{1}(\text{PF}_6)_2$  ( $5 \times 10^{-5} \text{ M}$  in  $\text{CH}_3\text{CN}$ , 298 K) upon the addition of  $\text{Fe}(\text{ClO}_4)_3$ .

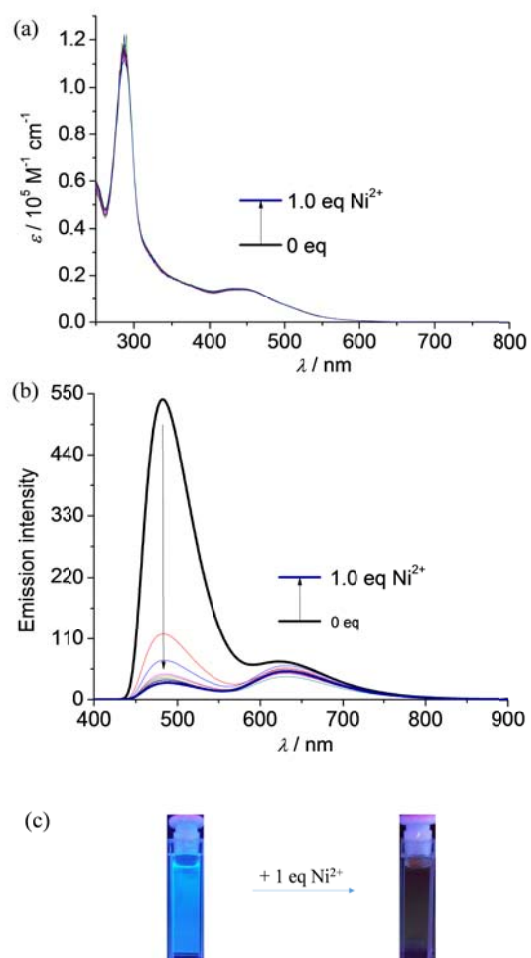


**Figure S16.** (a) Absorption spectral, (b) emission spectral, and (c) emission color (under 365 nm irradiation) changes of **1**(PF<sub>6</sub>)<sub>2</sub> ( $5 \times 10^{-5}$  M in CH<sub>3</sub>CN, 298 K) upon the addition of Ni(ClO<sub>4</sub>)<sub>2</sub>.

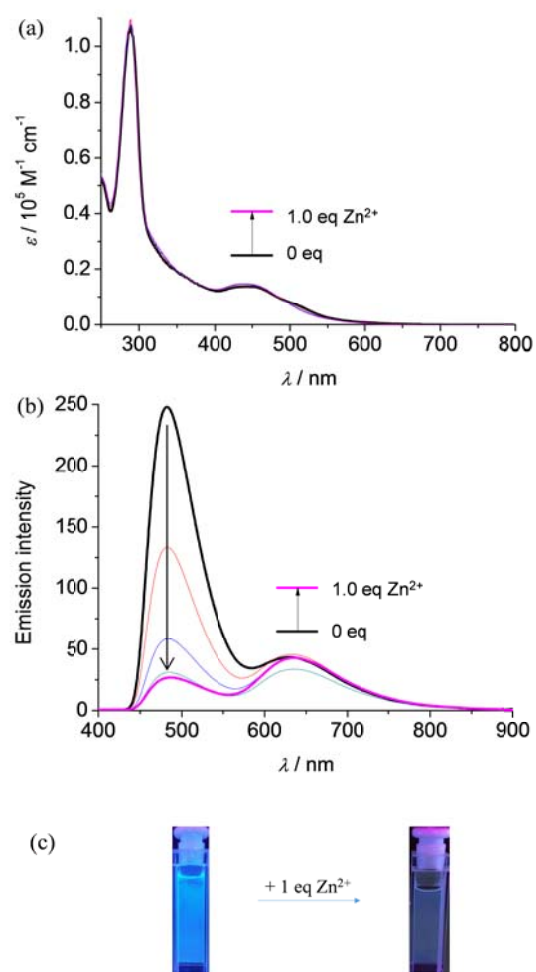


**Figure S17.** (a) Absorption spectral, (b) emission spectral, and (c) emission color (under 365 nm irradiation) changes of  $\mathbf{1}(\text{PF}_6)_2$  ( $5 \times 10^{-5} \text{ M}$  in  $\text{CH}_3\text{CN}$ , 298 K) upon the addition of  $\text{Zn}(\text{ClO}_4)_2$ .

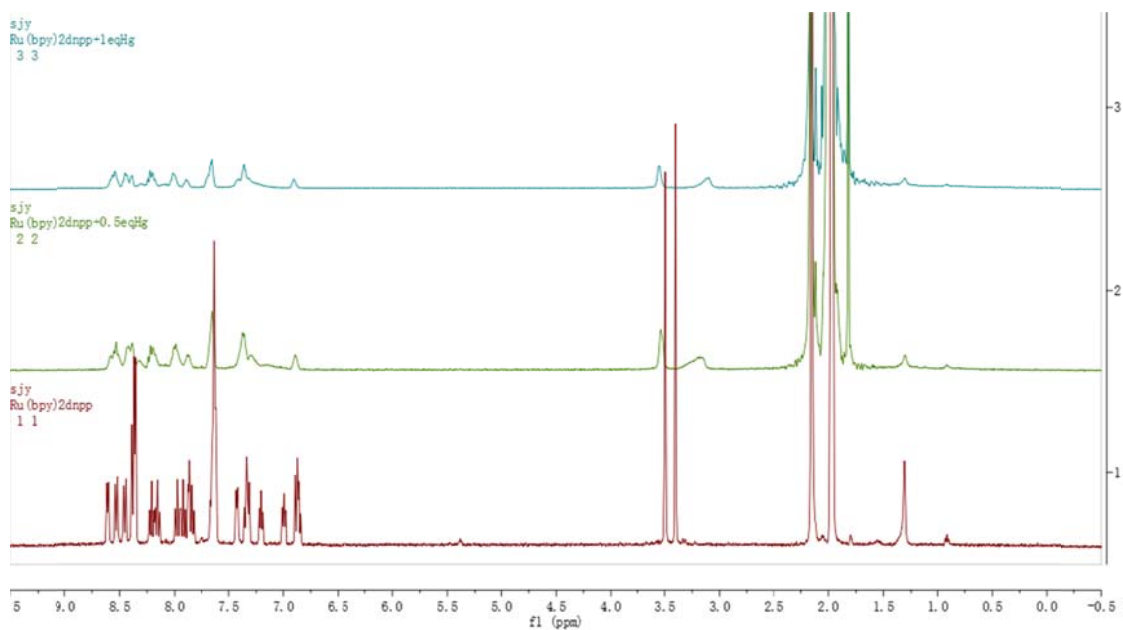


**Figure S18.**  $^1\text{H}$  NMR spectral changes of  $\mathbf{1}(\text{PF}_6)_2$  in  $\text{CD}_3\text{CN}$  upon the addition of 0.5 (middle) or 1.0 equiv (upper) of  $\text{Hg}(\text{ClO}_4)_2$ .

## 6. DFT and TDDFT Calculations

DFT calculations were carried out by using the B3LYP exchange correlation functional<sup>3</sup> and implemented in the Gaussian 09 package.<sup>4</sup> The input files were generated from the single-crystal X-ray data. The electronic structures were optimized with a general basis set with the Los Alamos effective core potential LANL2DZ basis set for Ru and 6-31G\* for other atoms.<sup>5</sup> The solvation effects in CH<sub>3</sub>CN were included for all calculations. No symmetry constraints were used in the optimization (nosymm keyword was used). Frequency calculations were performed with the same level of theory to ensure the optimized geometries to be local minima. All orbitals were computed at an isovalue of 0.03 e bohr<sup>-3</sup>. TDDFT calculations were performed on the DFT-optimized structures on the same level of theory.

---

<sup>3</sup> Lee, C.; Yang, W.; Parr, R. G. *Phys. Rev. B* **1988**, *37*, 785.

<sup>4</sup> Frisch, M. J.; Trucks, G. W.; Schlegel, H. B.; Scuseria, G. E.; Robb, M. A.; Cheeseman, J. R.; Montgomery, J. A.; Vreven, Jr. T.; Kudin, K. N.; Burant, J. C.; Millam, J. M.; Iyengar, S. S.; Tomasi, J.; Barone, V.; Mennucci, B.; Cossi, M.; Scalmani, G.; Rega, N.; Petersson, G. A.; Nakatsuji, H.; Hada, M.; Ehara, M.; Toyota, K.; Fukuda, R.; Hasegawa, J.; Ishida, M.; Nakajima, T.; Honda, Y.; Kitao, O.; Nakai, H.; Klene, M.; Li, X.; Knox, J. E.; Hratchian, H. P.; Cross, J. B.; Adamo, C.; Jaramillo, J.; Gomperts, R.; Stratmann, R. E.; Yazyev, O.; Austin, A. J.; Cammi, R.; Pomelli, C.; Ochterski, J. W.; Ayala, P. Y.; Morokuma, K.; Voth, G. A.; Salvador, P.; Dannenberg, J. J.; Zakrzewski, V. G.; Dapprich, S.; Daniels, A. D.; Strain, M. C.; Farkas, O.; Malick, D. K.; Rabuck, A. D.; Raghavachari, K.; Foresman, J. B.; Ortiz, J. V.; Cui, Q.; Baboul, A. G.; Clifford, S.; Cioslowski, J.; Stefanov, B. B.; Liu, G.; Liashenko, A.; Piskorz, P.; Komaromi, I.; Martin, R. L.; Fox, D. J.; Keith, T.; Al-Laham, M. A.; Peng, C. Y.; Nanayakkara, A.; Challacombe, M.; Gill, P. M. W.; Johnson, B.; Chen, W.; Wong, M. W.; Gonzalez, C.; Pople, J. A. *Gaussian 09*, revision A.2; Gaussian, Inc.: Wallingford CT, 2009.

<sup>5</sup> (a) Dunning, T. H.; Hay, P. J. In *Modern Theoretical Chemistry*; Schaefer, H. F., Ed.; Plenum: New York, 1976; Vol. 3, p 1. (b) Hay, P. J.; Wadt, W. R. *J. Chem. Phys.* **1985**, *82*, 299.

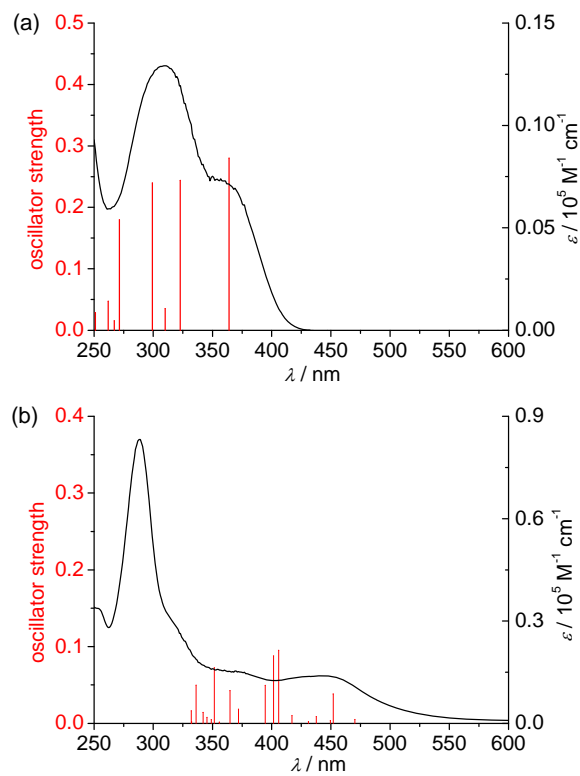


**Figure S19.** TDDFT-predicted excitations (red lines) of (a) dapz and (b)  $1^{2+}$ . The absorption spectra of dapz and  $1(\text{PF}_6)_2$  (black curves) are included for comparison.

**Table S4.** TDDFT results.<sup>a</sup>

Complex	$S_n$	$E$ [eV]	$\lambda$ [nm]	$f$	Dominant transition(s) (percentage contribution <sup>b</sup> )	assignment <sup>c</sup>
<b>dapz</b>	1	3.41	364	0.283	HOMO $\rightarrow$ LUMO (98%)	ILCT
	2	3.85	322	0.2441	HOMO $\rightarrow$ LUMO+1 (96%)	ILCT
	3	4.00	310	0.0354	HOMO $\rightarrow$ LUMO+2 (88%)	ILCT
	5	4.15	299	0.2399	HOMO $\rightarrow$ LUMO+3 (96%)	ILCT
	6	4.58	271	0.1799	HOMO $\rightarrow$ LUMO+4 (92%)	ILCT
	7	4.65	267	0.0155	HOMO-2 $\rightarrow$ LUMO (65%)	$\pi \rightarrow \pi^*$
	8	4.74	262	0.0473	HOMO-1 $\rightarrow$ LUMO+1 (76%)	$\pi \rightarrow \pi^*$
	9	4.95	251	0.0288	HOMO-1 $\rightarrow$ LUMO+2 (73%)	$\pi \rightarrow \pi^*$
	<b>1<sup>2+</sup></b>	2	2.75	452	0.0384	HOMO-1 $\rightarrow$ LUMO+1 (44%) HOMO-2 $\rightarrow$ LUMO+11 (41%)
7		3.06	406	0.0952	HOMO-2 $\rightarrow$ LUMO (52%)	ML <sub>bpy</sub> CT
8		3.09	401	0.0879	HOMO $\rightarrow$ LUMO+2 (88%)	ILCT(dapz)
9		3.15	395	0.0497	HOMO-3 $\rightarrow$ LUMO (22%) HOMO-3 $\rightarrow$ LUMO+1 (35%)	ML <sub>bpy</sub> CT
10		3.33	372	0.0184	HOMO-2 $\rightarrow$ LUMO+2 (47%) HOMO-1 $\rightarrow$ LUMO+2 (33%)	ML <sub>pyrazine</sub> CT
11		3.40	365	0.0425	HOMO-2 $\rightarrow$ LUMO+2 (45%) HOMO-1 $\rightarrow$ LUMO+2 (39%)	ML <sub>pyrazine</sub> CT ML <sub>pyrazine</sub> CT
13		3.53	351	0.0726	HOMO-3 $\rightarrow$ LUMO+2 (34%) HOMO $\rightarrow$ LUMO+3 (33%)	ML <sub>pyrazine</sub> CT L <sub>dapz</sub> L <sub>bpy</sub> CT
17		3.69	336	0.0498	HOMO-3 $\rightarrow$ LUMO+11 (28%) HOMO-3 $\rightarrow$ LUMO+12 (10%) HOMO $\rightarrow$ LUMO+3 (13%)	MC MC L <sub>dapz</sub> L <sub>bpy</sub> CT
19		3.75	331	0.0163	HOMO $\rightarrow$ LUMO+4 (19%) HOMO-2 $\rightarrow$ LUMO+3 (17%) HOMO-1 $\rightarrow$ LUMO+3 (33%)	ILCT(dapz) ML <sub>bpy</sub> CT ML <sub>bpy</sub> CT
					HOMO $\rightarrow$ LUMO+5 (26%)	L <sub>dapz</sub> L <sub>bpy</sub> CT

<sup>a</sup>Molecular orbitals are shown in Figures S17 and S18.

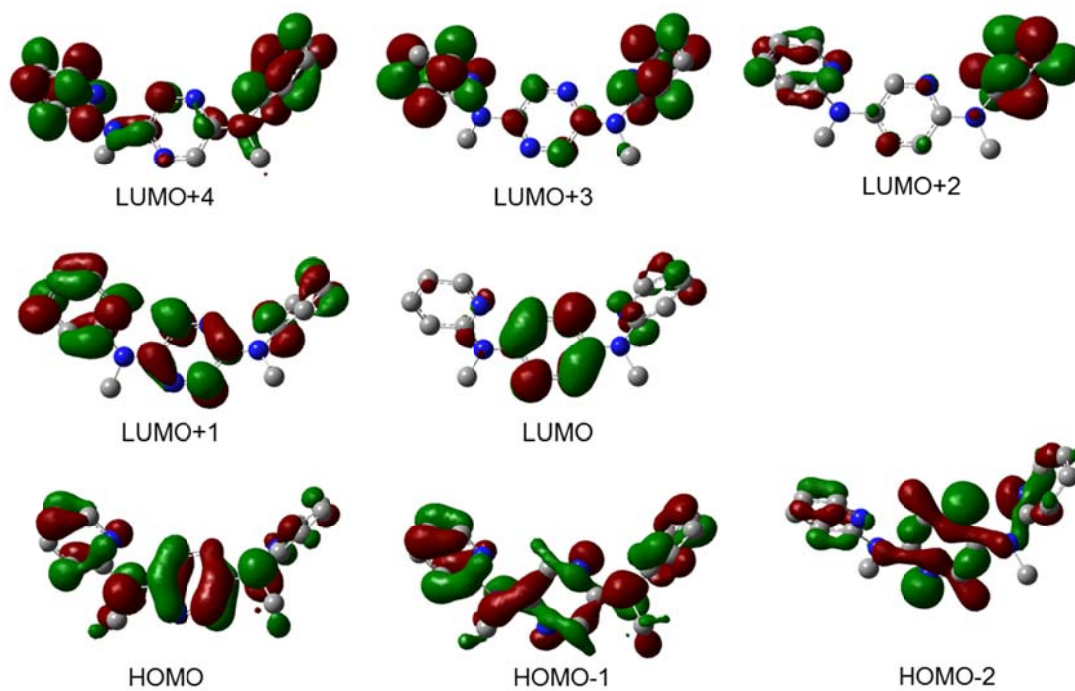


**Figure S20.** Isodensity plots of frontier molecular orbitals of dapz. All orbitals were computed at an isovalue of 0.03.

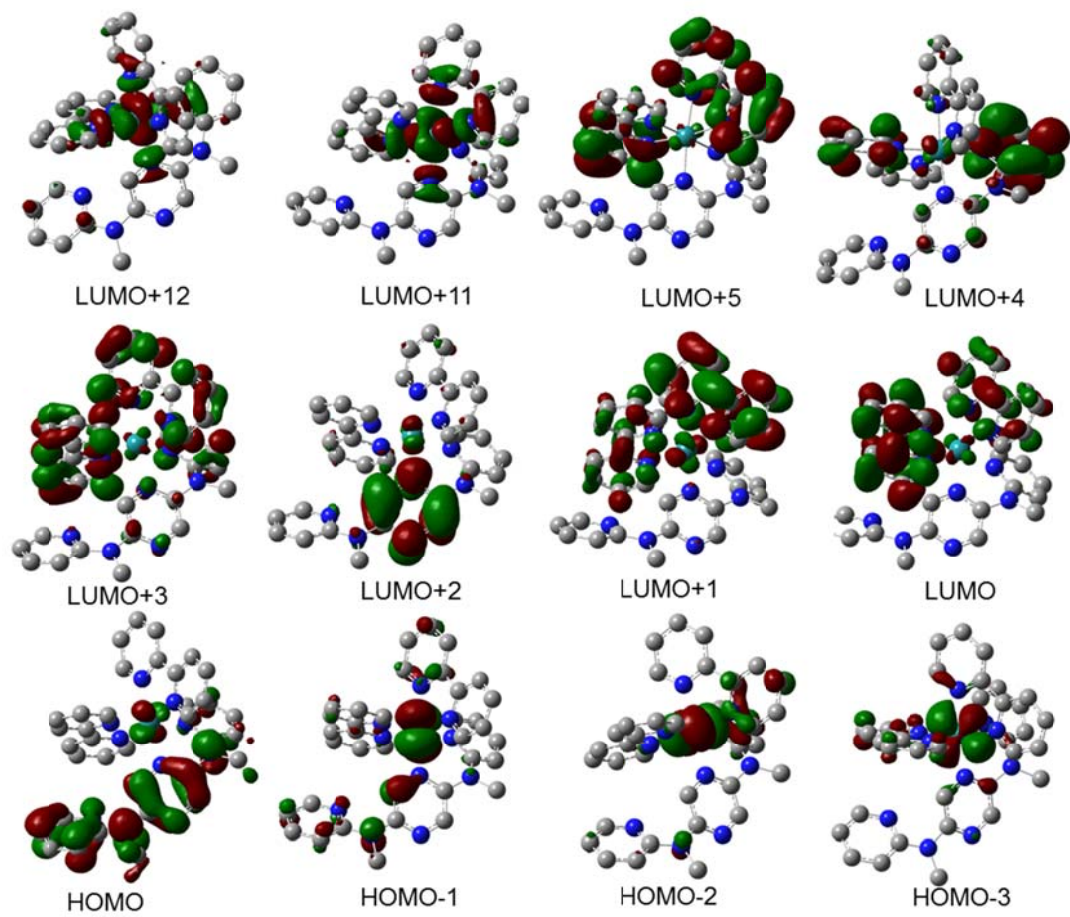


**Figure S21.** Isodensity plots of frontier molecular orbitals of  $1^{2+}$ . All orbitals were computed at an isovalue of 0.03.

## 7. Electrochemical Measurements

All electrochemical measurements were taken using a CHI 660D potentiostat with one-compartment electrochemical cell under an atmosphere of nitrogen. All measurements were carried out in CH<sub>3</sub>CN containing 0.1 M <sup>t</sup>Bu<sub>4</sub>NClO<sub>4</sub> as the supporting electrolyte at a scan rate of 100 mV/s (for cyclic voltammetry). The working electrode was a glassy carbon disk electrode (d = 3 mm). The electrode was polished prior to use with 0.05 μm alumina and rinsed thoroughly with water and acetone. A large area platinum wire coil was used as the counter electrode. All potentials are referenced to Ag/AgCl electrode in saturated aqueous NaCl without compensation for the liquid junction potential. Potentials vs ferrocene<sup>+0</sup> can be deduced by subtracting 0.45 V.

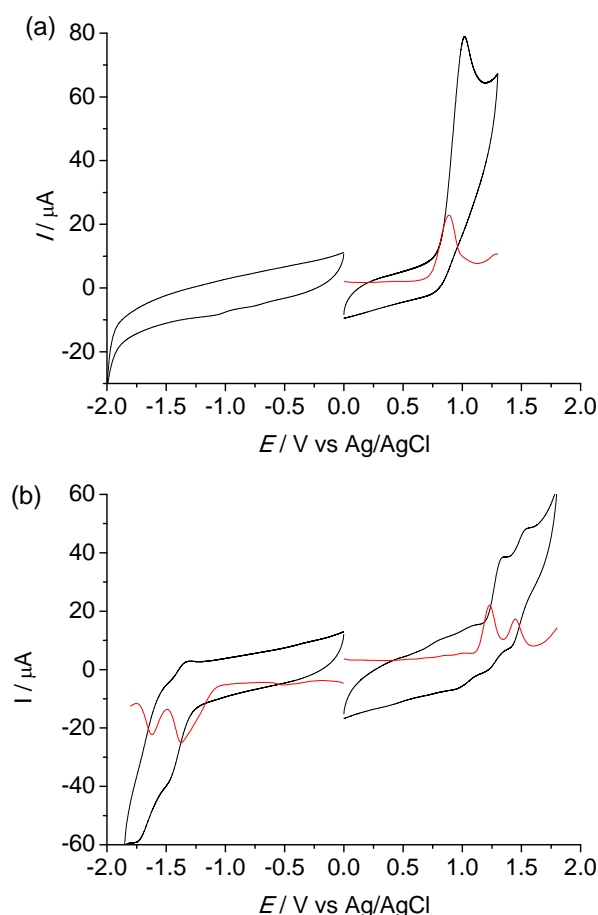


**Figure S22.** Cyclic voltammograms (black curves) and differential pulse voltammograms (red curves) of (a) dapz and (b) **1**(PF<sub>6</sub>)<sub>2</sub> in 0.1 M Bu<sub>4</sub>NClO<sub>4</sub>/CH<sub>3</sub>CN at a scan rate of 100 mVs<sup>-1</sup>.